Regulation of K^+ Flow by a Ring of Negative Charges in the Outer Pore of BK_{Ca} Channels. Part I: Aspartate 292 modulates K^+ Conduction by External Surface Charge Effect

Trude Haug,[1] Daniel Sigg,[5] Sergio Ciani,[2] Ligia Toro,[1,3,4] Enrico Stefani,[1,2,4] and Riccardo Olcese[1,4]

[1]Department of Anesthesiology-Division of Molecular Medicine, [2]Department of Physiology, [3]Department of Molecular and Medical Pharmacology, and [4]Brain Research Institute, David Geffen School of Medicine, University of California, Los Angeles, Los Angeles, CA 90095

[5]Department of Nuclear Medicine, VA Greater Los Angeles Healthcare System, Los Angeles, CA 90073

ABSTRACT The pore region of the majority of K^+ channels contains the highly conserved GYGD sequence, known as the K^+ channel signature sequence, where the GYG is critical for K^+ selectivity (Heginbotham, L., T. Abramson, and R. MacKinnon. 1992. *Science.* 258:1152–1155). Exchanging the aspartate residue with asparagine in this sequence abolishes ionic conductance of the *Shaker* K^+ channel (D447N) (Hurst, R.S., L. Toro, and E. Stefani. 1996. *FEBS Lett.* 388:59–65). In contrast, we found that the corresponding mutation (D292N) in the pore forming α subunit (hSlo) of the voltage- and Ca^{2+}-activated K^+ channel (BK_{Ca}, MaxiK) did not prevent conduction but reduced single channel conductance. We have investigated the role of outer pore negative charges in ion conduction (this paper) and channel gating (Haug, T., R. Olcese, T. Ligia, and E. Stefani. 2004. *J. Gen Physiol.* 124: 185–197). In symmetrical 120 mM [K^+], the D292N mutation reduced the outward single channel conductance by ~40% and nearly abolished inward K^+ flow (outward rectification). This rectification was partially relieved by increasing the external K^+ concentration to 700 mM. Small inward currents were resolved by introducing an additional mutation (R207Q) that greatly increases the open probability of the channel. A four-state multi-ion pore model that incorporates the effects of surface charge was used to simulate the essential properties of channel conduction. The conduction properties of the mutant channel (D292N) could be predicted by a simple ~8.5-fold reduction of the surface charge density without altering any other parameter. These results indicate that the aspartate residue in the BK_{Ca} pore plays a key role in conduction and suggest that the pore structure is not affected by the mutation. We speculate that the negative charge strongly accumulates K^+ in the outer vestibule close to the selectivity filter, thus increasing the rate of ion entry into the pore.

KEY WORDS: MaxiK channel • conduction • permeation • surface charge • Markov model

The Journal of General Physiology

INTRODUCTION

Early biophysical work explained ion selectivity and conductance in K^+ channels by a multi-ion single file pore containing more than one ion binding site (Neyton and Miller, 1988a; Neyton and Miller, 1988b; Harris et al., 1998; Hille, 2001). This initial hypothesis of a K^+ channel pore with multiple K^+ binding was directly visualized after resolving the crystal structure of bacterial K^+ channels (Doyle et al., 1998; Zhou et al., 2001; Jiang et al., 2003) and has been recently supported by molecular dynamics (MD) simulation (Berneche and Roux, 2001; Berneche and Roux, 2003; Capener et al., 2003). Although the amino acid sequence of the pore forming α subunit of the BK_{Ca} channel shows high similarity with other K^+ selective channels (Adelman et al., 1992; Butler et al., 1993; Wallner et al., 1995; Brelidze et al., 2003; Shealy et al., 2003; Nimigean et al., 2003), it conducts K^+ ~20-fold better (200–300 pS vs. 5–15 pS) while maintaining a high selectivity for K^+ (Latorre et al., 1989). Recent work demonstrates that negatively charged residues in the inner vestibule of the mammalian BK_{Ca} (mSlo) channel pore contribute to its high conductance. The neutralization of these negative charges in the mSlo channel (E321N/E324N) produces a two-fold reduction in single channel conductance (Brelidze et al., 2003; Nimigean et al., 2003). Accordingly, K^+ channels with smaller conductances (i.e., KcsA and *Shaker*) lack negative charges at equivalent positions. Thus, one would expect that negatively charged residues in the outer vestibule could also be involved in K^+ con-

Address correspondence to Riccardo Olcese, Dept. of Anesthesiology, Division of Molecular Medicine, BH-570 CHS, David Geffen School of Medicine, Box 95711, University of California, Los Angeles, Los Angeles, CA 90095-7115. Fax: (310) 206-1947; email: rolcese@ucla.edu

T. Haug's present address is Dept. of Molecular Biosciences, University of Oslo, NO-0316 Oslo, Norway.

Abbreviations used in this paper: MD, molecular dynamics; PMF, potential of mean force; WT, wild-type.

duction, and the higher conductance in BK_{Ca} channels could be related to the affinity and relative positions of the K^+ binding sites in the conduction pathway and/or to the existence of a higher density of K^+ ions due to a unique arrangement of negative charges in the vestibules.

The conserved signature sequence of K^+ channels, GYG, is believed to form the narrowest part of the pore and is responsible for the K^+ selectivity (Fig. 1) (Heginbotham et al., 1992). An alignment of the pore sequence of hSlo and *Shaker* channels shows a considerable similarity between the two K^+ channels, including the aspartate (D) immediately following the GYG sequence. In the tetrameric structure of the channel, the four aspartates form a ring of negative charges lining the outer pore (Fig. 1, A and B). The neutralization of the D in the *Shaker* channel and other Kv channels abolishes conduction (Hurst et al., 1996; Molina et al., 1998). In this and the following paper we have determined the role of the corresponding negative residue (D292) in the human BK_{Ca} α subunit (hSlo) (Wallner et al., 1995) in K^+ conduction, channel opening, and charge movement. We found that the neutralization of D292 (D292N) reduces the amplitude of the single channel current, introducing a prominent outward rectification, likely as a consequence of a reduced surface charge density. The same mutation also altered charge movement and the stability of the open state. The reduction in channel conductance by the D292N mutation suggests that this negative residue, pointing away from the selectivity filter (Doyle et al., 1998), is involved in conduction, probably by promoting a higher density of K^+ ions in the outer vestibule.

Over the last few years, much new information on the structure of K^+ channel pores has become available. High resolution X-ray crystallography has revealed five discrete binding sites for K^+ within the selectivity filter. Independent confirmation of the location of these K^+ binding sites was provided by all-atom molecular dynamic simulations, in which a detailed free energy landscape of the permeation pathway was determined by umbrella sampling (Berneche and Roux, 2001, 2003). The energy landscape contains modest free energy barriers, allowing, in theory, the reduction of a complete multi-ion permeation pathway to a manageable number of discrete states. We propose a phenomenological model that is consistent with the basic physical properties of the K^+ pore acquired from crystallographic and molecular dynamics data (Berneche and Roux, 2001, 2003; Zhou et al., 2001). The model incorporates the effect of surface charge at the mouth of the outer pore. We propose that negative surface charge generated by the D292 residue increases the local K^+ concentration at the outer pore with respect to bulk, thus maintaining a high conductance level even in the face of low bulk $[K^+]$. Neutralizing the surface charge contribution by D292 should reduce the local K^+ concentration, and consequently the K^+ conductance.

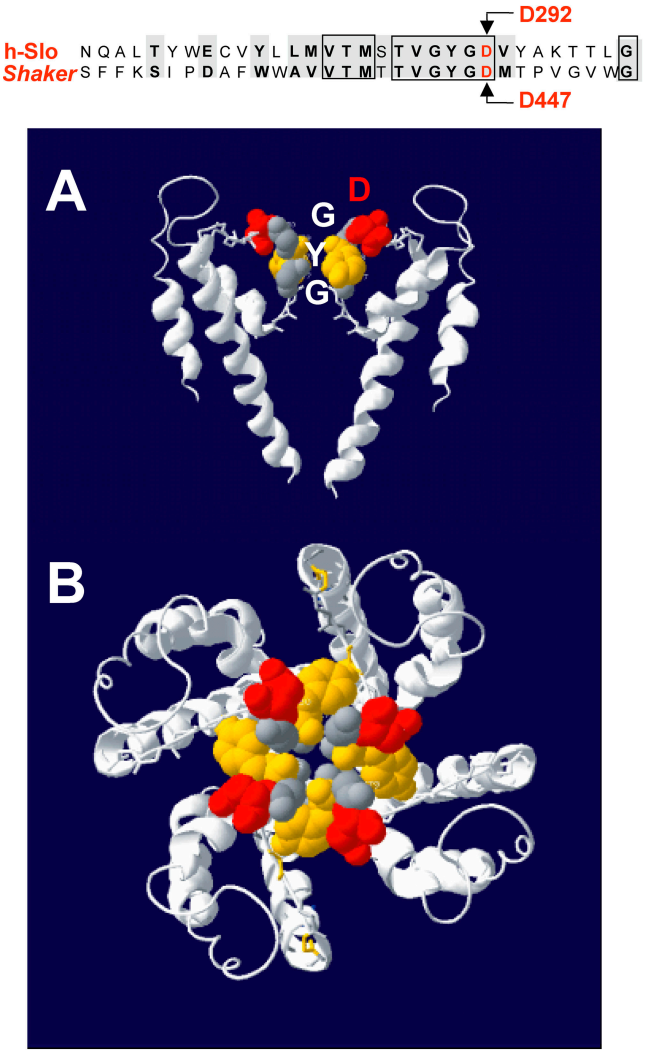

FIGURE 1. The D292N mutation neutralizes the negatively charged aspartic acid in the GYGD selectivity filter of the pore. The top panel shows the amino acid sequence alignment corresponding to the pore regions of hSlo and *Shaker* K^+ channels. The boxes enclose identical amino acids, while gray background shows residues with conserved properties. (A) Two of the four monomers that constitute a functional K^+ channel based on the crystal structure of KcsA proposed by Doyle et al. (1998). A probable arrangement of the conserved sequence of the pore region corresponding to the selectivity filter is shown. (B) The arrangement of all four monomers viewed from the top, revealing the central pore of the conduction pathway and the position of the four aspartates (red) lining the pore vestibule.

MATERIALS AND METHODS

Molecular Biology, Oocyte Preparation, and cRNA Injection

The following cDNAs were used for measurements of ionic and gating currents: hSlo (Wallner et al., 1995), hSlo-D292N, hSlo-R207Q, and hSlo-R207Q-D292N. The cDNAs were translated in

vitro (mMESSAGE mMACHINE; Ambion), and the cRNA was injected into *Xenopus laevis* oocytes (stage V–VI). 24 h before cRNA injection, the oocytes were treated with collagenase (200 U/ml; GIBCO BRL) in a Ca^{2+}-free solution in order to remove the follicular layer. Oocytes were injected with 50 nl cRNA (0.02–0.2 μg/μl) using a Drummond "nano-injector," and maintained at 18°C in modified Barth's solution containing (mM) 100 NaCl, 2 KCl, 1.8 $CaCl_2$, 1 $MgCl_2$, 5 Na-HEPES (pH 7.6), and 50 mg/ml gentamycin.

Solutions, Electrophysiological Recordings, and Analysis

Recordings were performed with conventional patch clamp techniques in the inside-out patch configuration. Membrane patches were made after removal of the vitellin membrane; macroscopic and single channel currents were recorded in symmetrical solutions containing (mM) 115 KMES, 5 KCl, 10 HEPES (pH 7.0). In this solution, the contaminant Ca^{2+} was ~6 μM. Free Ca^{2+} was measured with a Ca^{2+} electrode (World Precision Instruments). For the single channel experiments in varying symmetrical K^+ concentrations, external and internal solutions contained (mM) 5 KCl and 10 HEPES and various KMES concentrations to reach the desired K^+ concentration (pH 7.0). The pipette resistance for single channel measurements was 10–60 MΩ, and for macroscopic current measurements 1–3 MΩ. All experiments were performed at room temperature (22–24°C). The filter cut-off frequency was 1/5 of the sampling frequency. Values are reported as mean ± SEM.

Single channel current amplitudes were measured directly from single channel activity recorded in excised patches containing one or a few channels, during different voltage pulses. The average amplitudes at each voltage were estimated from several full channel openings.

Simulation of Permeation Properties

Based on the free energy landscape of KcsA conduction computed by Berneche and Roux (2001, 2003), a reduced model of permeation in K^+ channels can exist with as few as four discrete states. We have constructed a cyclic model with four states representing the most stable ion pore configurations (see Fig. 6 A). Occupancy of the pore varies from two to three ions at any given time. The transitions between doubly and triply occupied states are described by unimolecular rate constants, which are related to the energy description of the model via reaction rate theory (see APPENDIX). We have applied this model to conductance data obtained from patch clamp recordings of wild-type (WT) and mutant BK_{Ca} channels in a range of symmetric $[K^+]$.

The fitting of experimental data from hSlo WT and the D292N pore mutant were performed using SCoP3.51 (Simulation Resources, Inc.) together with solver routines for linear analysis obtained from published numerical algorithms (Press et al., 1992). The fitting of WT and mutant channel I–V curves and the dependence of the unitary conductance on [K+] was performed simultaneously. Fitting was performed with least squares minimization. The only parameter allowed to vary between WT and mutant was the external surface charge density, while all other adjustable parameters were identical for WT and D292N channels.

RESULTS

The D292N Mutation Reduces Single Channel Conductance

Unlike what has been demonstrated for the *Shaker* pore mutant D447N (Hurst et al., 1996), the corresponding mutation in the hSlo pore (D292N) did not prevent ion conduction. Single channel recordings revealed a reduced unitary conductance when compared with WT hSlo channels. Fig. 2 shows representative single channel current recordings in symmetric 120 mM K^+ from excised membrane patches expressing hSlo (Fig. 2 A) and hSlo-D292N channels (Fig. 2 C) in the presence of contaminant Ca^{2+}. The corresponding single channel current–voltage (I–V) curves are shown in Fig. 2 (B and D). The I–V curve is practically linear for WT channels (Fig. 2 B), while the D292N mutant shows a reduction in the conductance and a strong rectification for positive potentials close to 0 mV. No channel activity was detected at potentials negative of the K^+ reversal potential (E_K) even in high internal Ca^{2+} concentration (up to 400 μM) and for E_K up to +80 mV (unpublished data). The single channel chord conductance of hSlo-D292N channels, measured between +50 mV and +100 mV in symmetrical 120 mM KMES, was 150 ± 1.9 pS (SEM, $n = 8$), which is ~60% of hSlo single channel conductance in the same conditions (244 ± 2.6 pS, $n = 5$).

The D292N Mutation Dramatically Reduces Inward K^+ Flow

To attempt resolving hSlo-D292N inward channel activity we initially pulsed to 100 mV to elicit long channel openings and measured tail currents during repolarizations to −60 mV (Fig. 3 A). In traces where the channels are open at the end of the 100-mV step we should be able to record channel activity at −60 mV. The recordings were performed using excised patches in symmetric 120 mM K^+ solutions with contaminant Ca^{2+}. WT channels showed clearly detectable inward single channel current at the instant of repolarization (Fig. 3 A, left). In contrast, in hSlo-D292N channels, openings upon repolarization were not detected, even when multiple channel openings occurred before the repolarizing pulse (Fig. 3 A, right). We explored the possibility that hSlo-D292N channel activity remained undetected because of an extremely fast closing rate undetectable at the sampling frequency (40 kHz) and filter (8 kHz) used for acquisition. To increase the detection level, we performed equivalent determinations using larger membrane patches displaying macroscopic currents. Fig. 3 B shows a prominent tail current for the hSlo channels (left panel), with similar peak amplitude at −100 mV as the steady-state current at +100 mV. hSlo-D292N channels in the same conditions showed a smaller and faster tail current amplitude, which was a small fraction of the outward current amplitude (Fig. 3 B, middle). No comparable currents were observed from control oocytes of the same batch (Fig. 3 B, right), indicating that the small tail current in hSlo-D292N is not due to endogenous channels. These observations indicate that hSlo-D292N channels can conduct inwardly, but at a much lower rate than outwardly. The lack of observable inward openings at the single

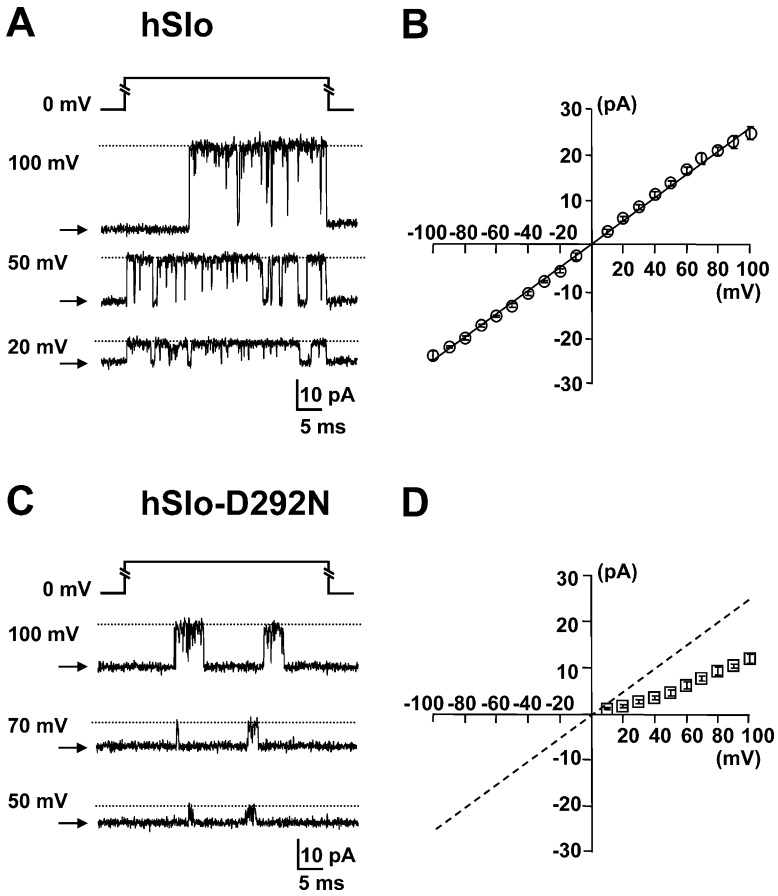

FIGURE 2. Single channel conductance reduction by the D292N mutation. Single channel currents were recorded from excised inside-out patches of *Xenopus* oocytes injected with hSlo (A) and hSlo-D292N (C). 40-ms voltage pulses to various potentials (numbers at left) were applied from 0-mV holding potential. The closed state indicated with arrows and the open channel current level is indicated with a dotted line. The recordings are done in symmetrical 120 mM K^+ solutions with contaminant Ca^{2+}. (B and D) Single channel I–V curves (hSlo, $n = 5$, and hSlo-D292N, $n = 7$). The outward conductance of the hSlo-D292N channel is approximately half of the conductance of the hSlo channel.

channel level can be explained by an extremely small single channel conductance and/or very brief channel openings.

Small Inward Channel Openings Can Be Resolved in the Double Mutant hSlo-R207Q-D292N

To increase the channel open time at negative potentials we used the R207Q mutation, which introduces a large negative shift (−200 mV in 1.7 μM $[Ca^{2+}]_i$) in the activation curve favoring long openings (Diaz et al., 1998). Fig. 4 shows channel recordings from inside-out patches in contaminant Ca^{2+} and symmetric 120 mM K^+ solutions for R207Q (A) and R207Q-D292N (B). In the double mutant, small channel openings were detected at negative potentials with a conductance markedly smaller than at positive potentials. The single channel I–V relationship (Fig. 4 B) is practically identical in WT hSlo and R207Q (Fig. 2 B), with a conductance of 245 ± 11.9 pS ($n = 4$). In the same condition, the D292N mutation reduced the outward conductance in the R207Q background in the same manner as in the WT hSlo (167 ± 0.9 pS, $n = 5$, measured between +50 and +100 mV). The hSlo-R207Q-D292N I–V curve illustrates a drastic reduction in single channel conductance for inward openings. We can conclude that the D292N mutation dramatically reduces channel conductance for inward openings, but does not abolish inward conduction completely.

The Outward Rectification in the hSlo-D292N Mutant Is Partially Relieved by Increasing Extracellular K^+ Concentration

The D292N mutation neutralizes a negative charge from the outer vestibule of the pore and reduces the outward conductance by ~40% and the inward conductance to a much greater extent. A conceivable explanation for these effects is a reduction of the local K^+ concentration in the outer pore close to the selectivity filter, due to the lack of the negatively charged residue. To explore this hypothesis, we obtained single channel I–V curves in hSlo and hSlo-D292N channels in symmetrical $[K^+]$ from 10 to 700 mM. Representative current traces and the corresponding I–V curves in 50, 200, and 700 mM K^+ are shown in Fig. 5 (A and C [hSlo] and B and E [hSlo-D292N]). In the D292N mutant in 700 mM symmetric K^+, channel openings could be detected at negative potentials, and the I–V curve showed a less marked rectification (Fig. 5, D and E). The average conductance between +50 and +100 mV of the WT and D292N channels are plotted versus the K^+ concentration in Fig. 5 F. The extrapolated single channel conductance to 0 K^+ tends to a finite value

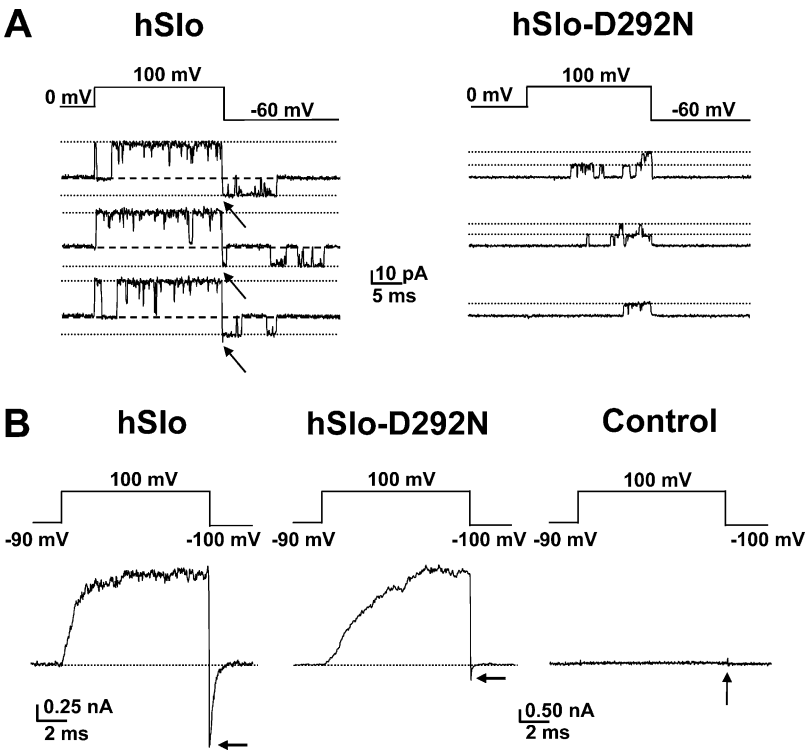

FIGURE 3. Drastic reduction of inward currents by the D292N mutation. (A) Current recordings from inside-out patches of oocytes expressing hSlo (left) and hSlo-D292N (right) channels. The voltage protocol is shown above the current traces. Note the lack of detectable single channel tail currents for the mutant channels (right). Linear components were subtracted using traces without channel openings. (B) Macroscopic current recordings from hSlo (left), hSlo-D292N (middle), and uninjected oocyte (right). The current was elicited by the voltage protocol shown above the traces, with a P/4 subtraction protocol from −90 mV subtracting holding potential. Note the smaller tail current amplitude of hSlo-D292N when compared with hSlo.

that is consistent with the presence of surface charges and predicted by the Gouy-Chapman theory. We have used the results from these experiments to set constraints on the energy landscape and surface charges in the permeation model that we fully describe in the next section.

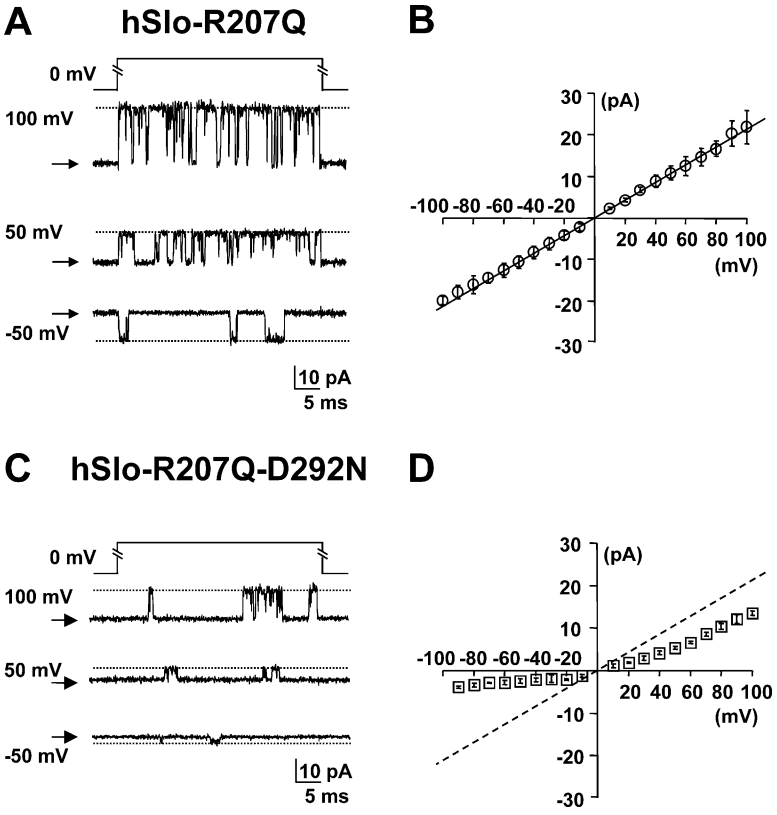

FIGURE 4. Detection of single channel openings in the hSlo-R207Q-D292N mutant. Single channel current recordings at selected potentials from inside-out patches in symmetrical 120 mM K^+ and contaminant Ca^{2+}. (A and B) hSlo-R207Q and hSlo-R207Q-D292N channel activity during 40-ms voltage pulses to various potentials from HP = 0 mV. Linear components were subtracted using traces without channel openings. The closed channel current level is indicated with arrows, and the open channel current level is indicated with a dotted line. Average single channel I–V curves for hSlo-R207Q (n = 3) and hSlo-R207Q-D292N (n = 5) are shown in B and D, respectively.

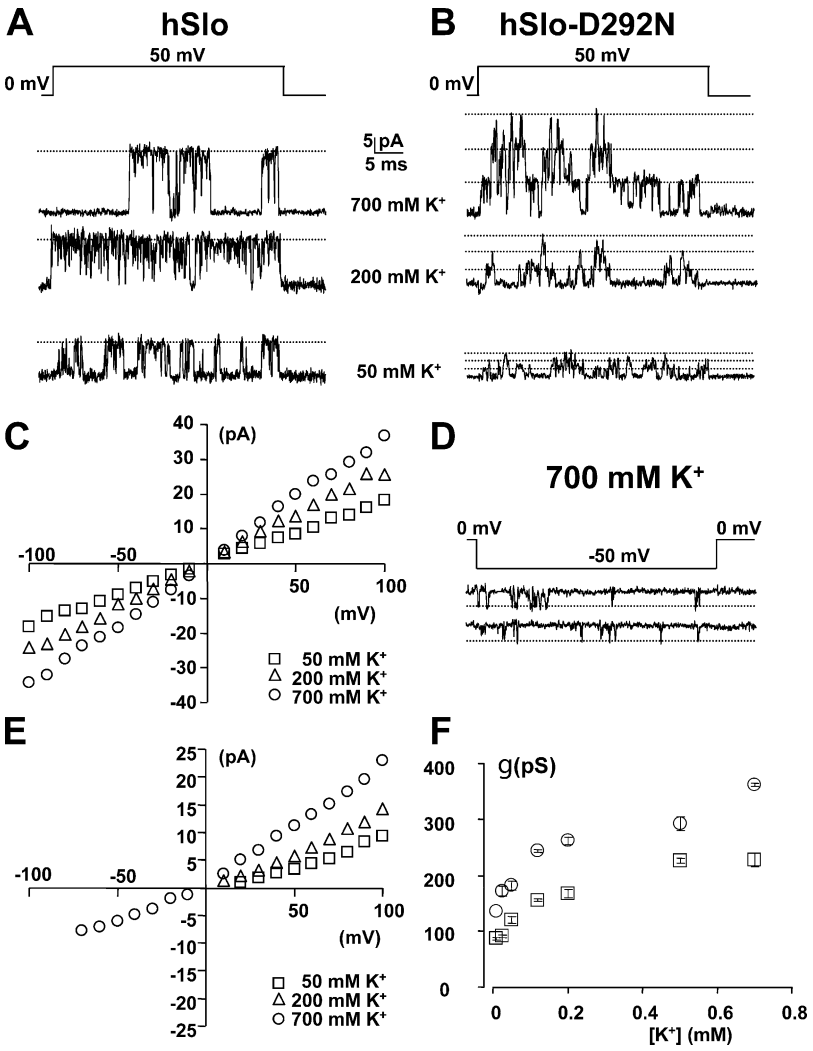

FIGURE 5. Effect of symmetric [K^+] on single channel conductance in hSlo and hSlo-D292N channels. Single channel current recordings from inside-out patches of oocytes expressing hSlo (A) and hSlo-D292N (B) are shown in various symmetrical [K^+] in contaminant Ca^{2+}. The current is elicited with 40-ms steps to +50 mV (A and B) and −50 mV (D) from 0-mV holding potential. The patch in B contains at least three channels. Note in D inward channel openings in hSlo-D292N at −50 mV and 700 mM symmetrical [K^+]. Linear components were subtracted using traces without channel openings. (C and E) Single channel I–V curves for hSlo and hSlo-D292N, respectively. No inward single channels were detected in hSlo-D292N in 50 (□) or 200 (△) mM K^+. (F) Single channel conductance vs. [K^+] plot for hSlo (○) and hSlo-D292N (□) channels. The single channel conductance was estimated from the linear range of the I–V relationship between +50 and +100 mV. The ionic strength of the solution was not kept constant, but increased with [K^+].

A Mechanism for the Change in Conduction Properties Observed in the D292N Mutant

We used single channel data at various K^+ concentrations to determine the free energy landscape of a four-state multi-ion permeation model for the BK_{Ca} channel pore (Fig. 6 A). In our reduced state model, we have adopted the following prominent features from recent molecular dynamics results (Berneche and Roux, 2001, 2003): (a) the pore possesses five K^+ binding sites; (b) during the permeation cycle, the occupancy of the pore varies between two and three ions; (c) there is concerted movement of ion pairs as they traverse the pore; and (d) the height of the free energy barriers are relatively modest (∼2 to 5 *kT*). As an additional feature, we implemented the Gouy-Chapman theory to simulate the effect of the charge neutralization (D292N) on the external surface charge density. The details of the calculations of current as a function of the model parameters are given in APPENDIX.

The parameters of the model were obtained by simultaneously fitting the single channel I–V curves (hSlo-D292N in symmetrical 120 mM and 700 mM K^+ and hSlo in symmetrical 120 mM and 500 mM K^+) and the conductance versus K^+ concentration curves (Fig. 6, C and D). The I–V relations (Fig. 6 C) were directly fit to the model, while the conductance versus K^+ concentration curves (Fig. 6 D) were fit after calculation of the chord conductance between +50 and +100 mV.

The experimental data for both WT and D292N could be accurately described using an identical model, but with an ∼8.6-fold reduction in the external surface charge density in the D292N mutation (WT = 0.0077 [$e^-/Å^2$], D292N = 0.0009 [$e^-/Å^2$]). This finding suggests that the difference in the conduction properties of the two pores can be explained by a reduction of the external surface charge density produced by the neutralization of D292. The fact that the energies of all the states and transitions (Fig. 6 B) could be maintained unchanged in the WT and mutant channels suggests that the pore structure remained unmodified by the mutation.

Fig. 6 C shows the four experimental single channel I–V curves superimposed to the theoretical I–V curves

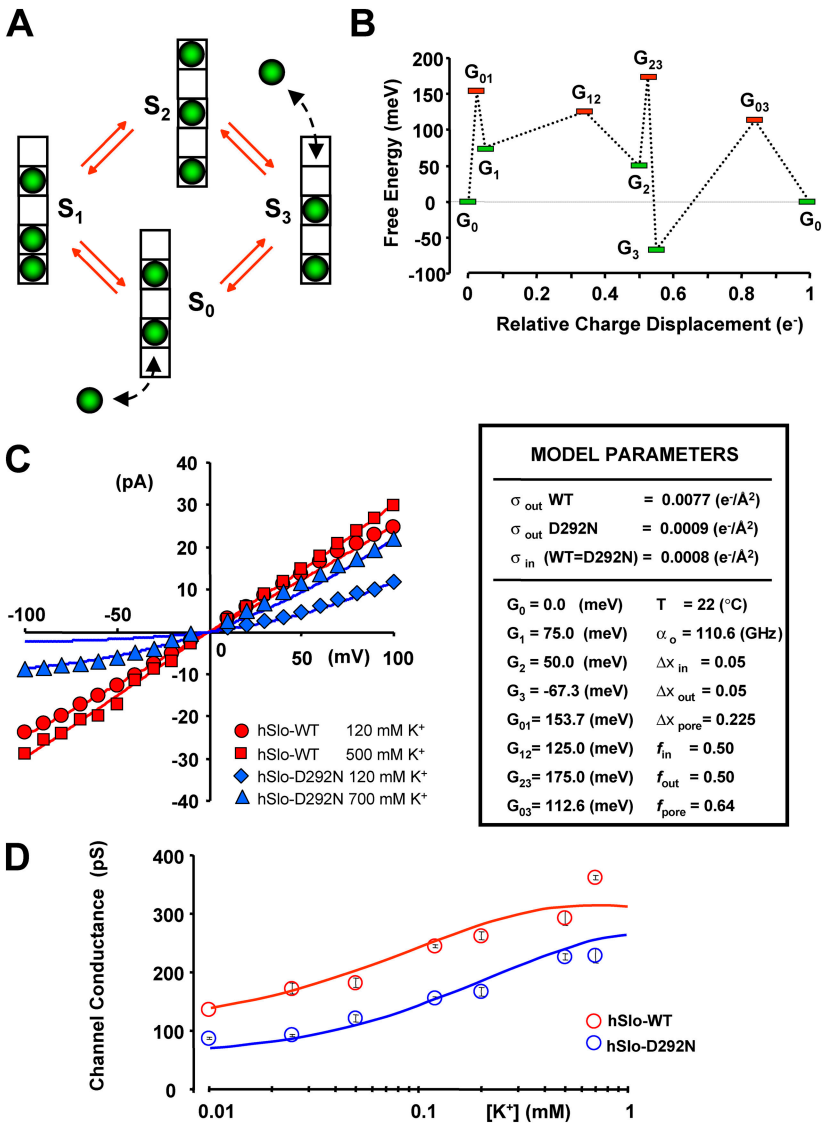

FIGURE 6. A conduction model for hSlo and hSlo-D292N channels. (A) State diagram for a cyclic four-state model illustrating the metastable states of pore occupancy. The selectivity filter contains five K^+ binding sites; K^+ ions are depicted as green spheres. (B) Schematic free energy landscape for both hSlo and hSlo-D292N channels in standard conditions (symmetric 120 mM K^+, no surface charge, and zero potential) during one permeation cycle. The landscape illustrates the free energy of the entire system "pore + ions" in different state of occupancy. The minima (G_{0-3}) are to the energies of the metastable states S_{0-3}. The maxima ($G_{01-12-23-03}$) are the transition energies. Results of model fitting to experimental data are shown in C and D. (C) Experimental (symbols) and fitted (lines) single channel I–V curves for WT hSlo (red) and hSlo-D292N (blue) at indicated symmetrical [K^+]. (D) Experimental (symbols) and fitted (lines) single channel chord conductance vs. [K^+] for hSlo (red) and hSlo-D292N (blue). The insert shows the model parameters. α_0 is the preexponential factor; G_{0-3} are the free energies of the states S_{0-3}; $G_{01-12-23-03}$ are the transition state energies; Δx_{in} and Δx_{out} are the fractional voltage drops on internal and external ion entry, respectively; Δx_{pore} is fractional voltage drops between two K^+ binding sites within the pore; σ_{out} and σ_{in} are the external and internal surface charge densities, respectively. f is the position of the transition barriers. See APPENDIX for detailed description of model parameters.

predicted by the model. Consistent with the neutralization of D292, the model is able to closely simulate the behavior of the hSlo WT channel and the hSlo-D292N mutant channel, solely by reducing the external surface charge density in the mutant. The model also accounts for the strong outward rectification of the mutant in symmetrical 120 mM K^+, as well as for the lessening of rectification observed when the K^+ concentration is increased (e.g., to 700 mM, Fig. 6 C). Increasing the K^+ concentration to 700 mM allowed detectable inward channel openings also in hSlo-D292N channels, indicating that higher [K^+] can compensate for the diminished local K^+ concentration after the neutralization of D292.

As expected with surface charge present, the single channel conductance as a function of the [K^+] tends to a finite value when the bulk ion concentration approached 0 (Fig. 6 D) (Bell and Miller, 1984; MacKinnon et al., 1989; Nimigean et al., 2003). This behavior, predicted by the Gouy-Chapman theory (McLaughlin, 1989) requires surface charge on both sides of the membrane. If charge is present on one side only, and the ion concentration in the solution is decreased on both sides, the theory predicts a smooth vanishing of the conductance when the permeant ion concentration goes to zero (Iino et al., 1997).

Assuming that the main contribution to the surface charge at the outer vestibule comes from the negative charges of D292, and that the area accessible to the selectivity filter is confined to a circular area of diameter 25 Å (Fig. 7 A) (Doyle et al., 1998), the corresponding surface charge density is ~0.008 $e^-/Å^2$, a value that is in agreement with that obtained from the fitting of experimental data to our model (0.077 $e^-/Å^2$).

DISCUSSION

The D292 residue in the hSlo pore region is part of the GYGD sequence, which is highly conserved among volt-

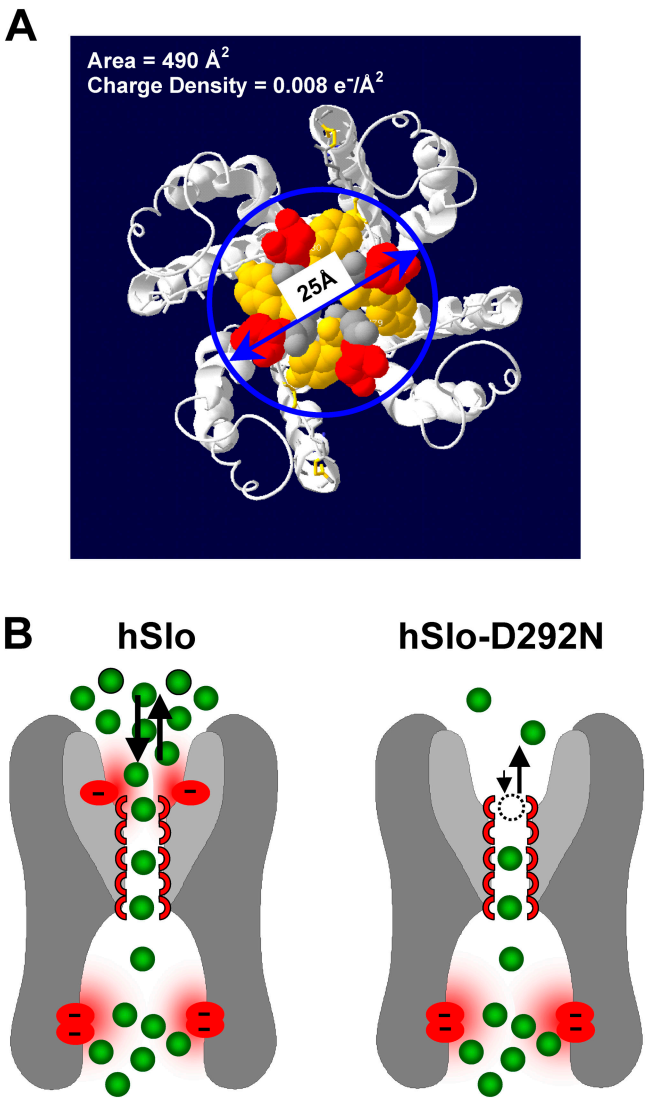

FIGURE 7. A molecular and functional model of the pore region. (A) Simple estimate of the surface charge density in hSlo by considering the area delimited by the circle (25 Å diameter). A surface charge density of ~0.008 e−/Å² can be estimated for the area including the four negative charges of the D292 residues. This value is very close to the fitted value of 0.0077 e−/Å². (B) Cartoon representation of the proposed role of D292 as a site for accumulating K^+ ions in the outer vestibule. The selectivity filter is depicted with five K^+ binding sites. The reduced [K^+] in the outer vestibule of hSlo-D292N results in reduced accessibility of K^+ to the outer binding site of the selectivity filter. Inner negative charge residues participating in ion conduction are shown at the bottom of the inner vestibule (Brelidze et al., 2003; Nimigean et al., 2003).

age-dependent potassium channels, and thus often referred to as the K^+ channel signature sequence (Heginbotham et al., 1994). When we replaced the negatively charged aspartate (D) with the neutral asparagine (N), the channel conductance for outward currents was reduced by ~40%, and displayed pronounced outward rectification, with a dramatic decrease of the channel inward conduction. Inward single channel openings could be detected only when the D292N mutation was combined with the R207Q mutation, which greatly increased the open probability (Fig. 4), or when the K^+ concentration was increased to 700 mM (Fig. 5). The lack of detectable inward currents at the single channel level in D292N is likely due to a combination of very small single channel amplitude and extremely short open time. In fact, when the open probability was significantly increased by the addition of the R207Q mutation (hSlo-R207Q-D292N), small and brief single channel openings were detected. However, the conductance at potentials negative to the E_K was only a fraction of the outward conductance. One explanation for the almost complete loss of inward conduction after the neutralization of D292 by N is that the ring of the four negative charges in the tetrameric structure of the channel, in close proximity of the selectivity filter, is crucial for a local accumulation of K^+ ions necessary for an efficient inward conduction. Nimigean et al. (2003) and Brelidze et al. (2003) have recently reported a similar reduction in single channel conductance when neutralizing negative charges (E321N/E324N) in the inner vestibule of the mSlo channel, proposing that these charges increase the K^+ concentration close to the intracellular entryway of the pore, thereby contributing to the large single channel conductance (Brelidze et al., 2003; Nimigean et al., 2003). K^+ channels with smaller conductance do not have negative charges in the equivalent position. Endowing KcsA channel with a negatively charged residue at the corresponding position (A108D) considerably increased the single channel conductance (Nimigean et al., 2003). The neutralization of negative charges on the external surface of the rat native BK_{Ca} channel using trimethyloxonium (TMO), a carboxyl group methylating reagent, reduced single channel conductance for both the outward and inward current without affecting ion selectivity (MacKinnon and Miller, 1989). In addition, TMO treatment introduced rectification properties qualitatively similar to those described for the D292N mutation, although they were much less pronounced and occurred only under low ionic strength conditions. One explanation for these observations is that negative charges on the outer face of the channel may enhance conduction by accumulating K^+ (MacKinnon et al., 1989). We have reached the same conclusion using site-directed mutagenesis to reduce the charges via neutralization of D292 by asparagine. Accordingly, in our simulation, we have been able to account for the effect on the conductance of the D to N mutation by simply decreasing the density of the external surface charge density. The observed ~40% decline of outward conductance can be explained by the reduction of surface charge in the outer vestibule, resulting in a smaller potential drop across the pore.

The role of this highly conserved residue in conduction and selectivity has also been investigated in other Kv channels (Goldstein et al., 1994; Kirsch et al., 1995; Aiyar et al., 1996; Molina et al., 1998; Chapman et al., 2001). These studies seemed to indicate that only charge-conservative mutations are tolerated for this residue, since charge-neutralizing mutations produced nonfunctional channels. When the charges were only partially neutralized by creating dimers of the Kv2.1 subunits and neutralizing only one of the two D (D378T) in each dimer, the resulting channel was functional (Kirsch et al., 1995), although the conductance was lower and also exhibited a marked outward rectification. However, conductance measurements at different ionic strengths did not support the idea that ion depletion due to screening of the surface potential is the main cause of the rectification. With the hypothesis that the negative charges in the outer vestibule might be arranged differently in BK_{Ca} channels than in other K^+ channels, one can speculate that the D292 contributes more to surface charge, and hence K^+ accumulation, than the corresponding residue in Kv2.1.

Interestingly, the conservative mutation D to E in both *Shaker* and Kv2.1 channels also altered channel properties by reducing the conductance, lowering the stability of the open state (Chapman et al., 2001), and increasing the rate of inactivation (Molina et al., 1998). These findings suggest that also the exact position of the negative charge is important, presumably both for K^+ accumulation and for the proposed structural contribution.

The reduction in limiting Po in the D292N channels could be related to a reduced K^+ concentration near the external pore. In fact, it is well established that K^+ channels collapse after eliminating K^+ ions from the pore (Almers and Armstrong, 1980). An accepted view is that K^+ stabilizes the open state by its occupancy of the pore. This scenario has been shown for different potassium channels including *Shaker* (Gomez-Lagunas, 1997; Loboda et al., 2001) and MaxiK channels (Vergara et al., 1999; Eghbali et al., 2002). Our results suggest that the conserved negatively charged aspartate (D) in the GYGD sequence powerfully accumulate K^+ in the external mouth, ensuring a high rate of K^+ entering the pore and stabilizing the open state.

Fig. 7 B shows a cartoon of hSlo and hSlo-D292N, depicting a possible scenario for K^+ binding and accumulation. D292 is indicated as a negative charge that strongly contributes to accumulation of K^+ close to the selectivity filter, enabling inward conductance. Neutralization of this "accumulation site" (D292N) drastically reduces the availability of K^+ for inward flux. The outward flux is less affected, as it would be expected, since at positive potential, the conductance is determined in large part by the internal K^+ concentration, which is unaltered by the mutation.

In conclusion, our data support the view that D292 in the hSlo pore acts as an accumulation site for K^+, allowing high conduction and a linear I–V relationship. At the same time, the high local $[K^+]$ could contribute to the stability of the open state. We have demonstrated that the lack of a stable open state in hSlo-D292N is also reflected by a reduction in the slow component of the gating charge, which has been associated to transition between open and closed states (Horrigan and Aldrich, 1999; Haug et al., 2004). The reduction in single channel conductance and the rectification that occurs upon neutralization of D292 can be simulated by decreasing the external surface charge density by a factor of $\sim$8.6, leaving the energy profiles for WT and D292N channels identical. Interestingly, the degree of reduction in surface charge density in D292N, estimated by fitting the data with the permeation model presented here, does not seem to be strictly dependent on the type of model used to describe conduction. In fact, using a simpler, yet unrealistic, model (with only two ion-binding sites), we were still able to accurately describe the properties of WT and mutant permeation. The striking commonality between these two very dissimilar models is that they both predicted not only the similar values for the surface charge density, but also the same degree of reduction in the external surface charge after neutralization of D292 (8.1-fold vs. 8.6-fold reduction; unpublished data). This result reinforces the view that the important feature for determining the changes in conduction properties of the mutant channel is not a function of the details of pore dynamics, but simply a property of the surface charge density. Also, the fact that unlike Kv channels, hSlo tolerates the fourfold neutralization of D292 suggests that this residue may have a different structural role in Kv and BK_{Ca} channels.

APPENDIX

The permeation model was developed according to the free energy landscape (potential of mean force [PMF]) of ion-pore dynamics constructed from MD simulations of a potassium channel pore (Berneche and Roux, 2001, 2003). The simulations predict modest energy barriers for ion translocation in the KcsA channel, suggesting that a discrete state Markov model may serve as a realistic representation of the "ion hopping" behavior that has been demonstrated in Brownian motion simulations (on a slower time scale than is typically achievable in MD) (Berneche and Roux, 2003). The Markovian states represent transiently stable (metastable) configurations of the pore and any residing ions. The state diagram (Fig. 6 A) is reversible and

cyclic. One ion equivalent is translocated through the pore for every full cycle. A one-dimensional representation of the free energy landscape traversed by the combined system (pore + ions) is illustrated in Fig. 6 B. The choice of "reaction coordinate" is the charge displacement (relative to an arbitrary starting value) recorded as the integral of the ionic current. It is a function of the positions of all pore-occupying ions along the pore potential profile (Roux, 1997). Thus, the PMF in Fig. 6 B describes the kinetics of the system as a whole, rather than the movement of any individual ion. Estimates of the value of unidirectional rate constants connecting adjacent minima (i.e., the metastable states) in the free energy landscape are theoretically obtained from mean first passage times across the separating barrier (Sigg and Bezanilla, 2003). Reaction rate theory specifies that rates over barriers at least several kT high can be approximated by an equation with the following form:

$$\alpha_{ij} = \alpha^{o}_{ij}\exp\left(\frac{-(\Delta G_{ij} - V\Delta q_{ij} - \alpha_i \Delta n_{ij})}{kT}\right). \tag{A1}$$

Transition energies enumerated in the exponent of Eq. A1 include ΔG_{ij}, the change in free energy; the canonical pairing of membrane potential (V) and charge displacement (Δq_{ij}); and the contribution of the chemical potential ($\mu = kT \ln C/C_{\text{ref}}$) of the bulk electrolyte solution on a change in the ion occupancy (n) of the pore. The quantity C is the activity of an ion species in solution, which we approximate by the bulk ionic concentration. The quantity kT has its usual thermodynamic significance of thermal energy and has a value of ~25 meV at room temperature.

In the absence of concentration and voltage gradients across the membrane (i.e., $\mu_{OUT} = \mu_{IN}$ and $V = 0$), the channel pore is in equilibrium with its surrounding heat and ion particle bath, implying that clockwise and counterclockwise circulation around the state diagram is equally likely. The zero-gradient equilibrium condition for the PMF landscape is automatically satisfied by assigning energy values (relative to the energy G_0 of state S_0) to the three remaining minima (G_{1-3}) and transition states (G_{ij}) and calculating the rate constants according to these values. In the presence of gradients, an ionic current $I = \Sigma_{ij} p_i \alpha_{ij} (\Delta q_{ij} - \Delta q_{ji})$, where p_i is the steady-state likelihood of state occupancy, is quickly established except in the particular case of the Nernst equilibrium condition ($V = kT/e_o \ln C_{out}/C_{in}$), in which case voltage and concentration gradients offset one another. Ensuring that the system satisfies the Nernst equilibrium while adjusting parameters (for example during a fitting process) requires careful bookkeeping that is most easily achieved with an energy description of the model rather than fitting rate constants directly. The explicit form of transition energies are given by the following matrices (indices from 0 to 3):

$$\{\Delta G\} = \begin{bmatrix} 0 & G_{01} - G_0 & 0 & G_{03} - G_0 \\ G_{01} - G_1 & 0 & G_{12} - G_1 & 0 \\ 0 & G_{12} - G_2 & 0 & G_{23} - G_2 \\ G_{03} - G_3 & 0 & G_{03} - G_3 & 0 \end{bmatrix}, \tag{A2}$$

$$\{V\Delta q\} = \tag{A3}$$

$$V\begin{bmatrix} 0 & f_i \Delta x_i e_o & 0 & -2(1-f_p)\Delta x_p e_o \\ -(1-f_i)\Delta x_i e_o & 0 & 2f_p \Delta x_p e_o & 0 \\ 0 & -2(1-f_p)\Delta x_p e_o & 0 & f_e \Delta x_e e_o \\ 2f_p \Delta x_p e_o & 0 & -(1-f_e)\Delta x_e e_o & 0 \end{bmatrix},$$

$$\{\alpha\Delta n\} = \begin{bmatrix} 0 & kT\ln(C_i/C_{ref}) & 0 & 0 \\ 0 & 0 & 0 & 0 \\ 0 & 0 & 0 & 0 \\ 0 & 0 & kT\ln(C_e/C_{ref}) & 0 \end{bmatrix}. \tag{A4}$$

Several quantities in the previous matrices require clarification. The variables Δx_{in}, Δx_{out}, and Δx_{pore} represent the fractional voltage drop experienced by an ion as it enters the selectivity region from the internal vestibule to the innermost binding site (Δx_{in}), from the extracellular solution to the outermost binding site (Δx_{out}), and while hopping among the five equally spaced binding sites within the selectivity region (Δx_{pore}). An ion experiences the full drop in applied voltage as it traverses from the internal vestibule to the extracellular solution. Therefore $\Delta x_{in} + \Delta x_{out} + 4\Delta x_{pore} = 1$. The similarly subscripted variables f_{in}, f_{out}, and f_{pore} define the location of the peak energy of an ion between adjacent binding sites as a fraction of the voltage drop between the sites. In the case of symmetric barriers, $f = 0.5$. Because state transitions are global events, the charge displacement matrix of Eq. A3 reflects the collective motion of the reaction coordinate rather than a single ion. For example, transitions S1 → S2 and S0 → S3 are characterized by the synchronous displacement of two ions in the selectivity filter. By assuming that the movement of the ion pair is tightly coupled, the value of f_{pore} assigned to the transition of the ion pair is equal to that of the single ion-hopping event. The purpose of the reference concentration C_{ref} in Eq. A4 was to scale the free energy contribution of the entry of an ion into the pore to make it comparable to other activation energies, since entry rates are linearly dependent on K^+ concentration. For symmetric solutions at concentration C_{ref} (arbitrarily chosen to be the physiological concentration of 120 mM), the chemical potential has no

effect on transition energies. Stated in a different way, transition energies for ion entry are presented with reference to the physiological concentration C_{ref}.

To model the effects of neutralizing charged residues near the mouth of the pore, we assumed that they contribute to a surface charge density as described by Gouy-Chapman theory. In a fast equilibrium, the ion concentration profiles near the membrane remain constant during permeation and are given by the Poisson-Boltzmann distribution. Given internal and external surface charge densities (σ_{in} and σ_{out}), the change to the effective membrane potential and ion concentrations at the solution/pore interfaces are given by $V' = V + \Psi_{in} - \Psi_{out}$, $C_{in}' = C_{in}\exp(\Psi_{in}e_o/kT)$, and $C_{out}' = C_{out}\exp(\Psi_{out}e_o/kT)$. These primed values ($V'$, C_{in}', and C_{out}') simply replace their bulk counterparts (when surface charge is present) in the expressions for transition energies described by Eqs. A1–A4 without altering the Nernst equilibrium condition. The external surface potential calculated from the Gouy-Chapman theory is $\Psi_{out} = (\sigma_{out}/|\sigma_{out}|)\ \ln\{1 + A_{out}/2C_{out} + [A_{out}/C_{out} + A_{out}^2/4C_{out}^2]^{1/2}\}$. A similar expression holds for the internal surface charge density. The quantity A_{out} is related to σ_{out} by $A_{out} = \sigma_{out}^2/2kT\varepsilon\varepsilon_o$, where ε is the dielectric constant of water ($\cong$78), and ε_o is the "permitivity of vacuum" ($5.53 \times 10^{-5}\ e_o\ mV^{-1}nm^{-1}$). A_{out} has dimensions of concentration, and if the surface charge density σ_{out} is expressed in units of $e_o/Å^2$, $A_{out} \approx (272\ \sigma_{out})^2$ moles/liter at room temperature.

The preexponential factor α^o_{ij} in equation A1 reflects the contributions of friction damping and entropic factors such as the shape of the free energy landscape leading to the transition state (Kramers, 1940). In a phenomenological description of permeation such as is presented here, there is a trade-off between the values of the preexponential factor and the transition energies that cannot be resolved without further information. Based on the evidence from the previously mentioned molecular dynamics studies that barrier heights in KcsA do not exceed 3–5 *kT*, we fixed the transition energy of the apparently rate-limiting step ΔG_{23} at 125 meV, and allowed the preexponential factor and other transition energies to vary. Preexponential factors were made equal in all transitions, in effect absorbing differences in landscape profiles and friction effects into the entropic component of the transition free energy. Because temperature or viscosity effects were not studied here, doing so caused no loss in generality. We attempted to keep transition barriers sufficiently large to justify the use of reaction rate theory to model the flow of ions through the pore (at least 50 meV = $\sim$2 *kT*). The discreteness of the ion distribution function based on simulated free energy profiles (Berneche and Roux, 2003) gives us some justification for pursuing the reduced state Markov model rather than using a more general but more computationally intensive electrodiffusion approach that requires more information than is available to us. Of note, the PMF profile shown in Fig. 6 B obtained after fitting our model to BK_{Ca} single channel currents differs qualitatively from the free energy profile of Berneche and Roux (2001) obtained from MD simulation of the KcsA pore. In particular, relative to S0, the energy of S3 (G3) in our model is significantly lower (by 2–3 *kT*) than the minimum energy region of the equivalent state in the two-dimensional energy landscape of KcsA permeation, and the barrier between S0 and S3 is larger in our model (by $\sim$4 *kT*). These differences may relate in part to variation among channels, failure to take into account changes in the diffusion coefficient, experimental error, or the use of an inappropriate model. A possible explanation for the lower energy of S3 in our model is that the range of motion of pore ions in the S3 configuration of KcsA is greater than in other configurations, thus lowering the relative free energy of the state in the one-dimensional representation through entropic means. Further studies, possibly involving structural information of the BK_{Ca} channel pore, will be useful in determining whether the pores of the two channels demonstrate similar dynamic behavior.

This work is dedicated to the memory of Professor Sergio Ciani (1938–2003), beloved friend and colleague.

We thank Ramon Latorre for insightful comments, Antonius VanDongen for the TRANSIT program for single channel kinetics analysis, Viktor Grabarchuk for developing the acquisition and analysis programs GPATCHW and ANALYSIS, and Evgenia Grigorova for the technical support with *Xenopus* oocytes.

This work was supported by National Institutes of Health grant NS43240 to R. Olcese, GM52203 to E. Stefani, and HL54970 to L. Toro, by the Norwegian Research Council grant 133604/410 to T. Haug, and by American Heart Association Grant in Aid 0250170N to R. Olcese.

Olaf S. Andersen served as editor.

Submitted: 22 September 2003
Accepted: 2 July 2004

REFERENCES

Adelman, J.P., K.Z. Shen, M.P. Kavanaugh, R.A. Warren, Y.N. Wu, A. Lagrutta, C.T. Bond, and R.A. North. 1992. Calcium-activated potassium channels expressed from cloned complementary DNAs. *Neuron.* 9:209–216.

Aiyar, J., J.P. Rizzi, G.A. Gutman, and K.G. Chandy. 1996. The signature sequence of voltage-gated potassium channels projects into the external vestibule. *J. Biol. Chem.* 271:31013–31016.

Almers, W., and C.M. Armstrong. 1980. Survival of K^+ permeability and gating currents in squid axons perfused with K^+-free media. *J. Gen. Physiol.* 75:61–78.

Bell, J.E., and C. Miller. 1984. Effects of phospholipid surface charge on ion conduction in the K+ channel of sarcoplasmic reticulum. *Biophys. J.* 45:279–287.

Berneche, S., and B. Roux. 2001. Energetics of ion conduction through the K^+ channel. *Nature.* 414:73–77.

Berneche, S., and B. Roux. 2003. A microscopic view of ion conduc-

tion through the K+ channel. *Proc. Natl. Acad. Sci. USA*. 100: 8644–8648.

Brelidze, T.I., X. Niu, and K.L. Magleby. 2003. A ring of eight conserved negatively charged amino acids doubles the conductance of BK channels and prevents inward rectification. *Proc. Natl. Acad. Sci. USA*. 100:9017–9022.

Butler, A., S. Tsunoda, D.P. McCobb, A. Wei, and L. Salkoff. 1993. *mSlo*, a complex mouse gene encoding "maxi" calcium-activated potassium channels. *Science*. 261:221–224.

Capener, C.E., P. Proks, F.M. Ashcroft, and M.S. Sansom. 2003. Filter flexibility in a mammalian K channel: models and simulations of Kir6.2 mutants. *Biophys. J.* 84:2345–2356.

Chapman, M.L., H.S. Krovetz, and A.M. VanDongen. 2001. GYGD pore motifs in neighbouring potassium channel subunits interact to determine ion selectivity. *J. Physiol.* 530:21–33.

Diaz, F., P. Meera, J. Amigo, E. Stefani, O. Alvarez, L. Toro, and R. Latorre. 1998. Role of the S4 segment in a voltage-dependent calcium-sensitive potassium (h*Slo*) channel. *J. Biol. Chem.* 273: 32430–32436.

Doyle, D.A., J.M. Cabral, R.A. Pfuetzner, A. Kuo, J.M. Gulbis, S.L. Cohen, B.T. Chait, and R. MacKinnon. 1998. The structure of the potassium channel: molecular basis of K+ conduction and selectivity. *Science*. 280:69–77.

Eghbali, M., R. Olcese, M.M. Zarei, L. Toro, and E. Stefani. 2002. External pore collapse as an inactivation mechanism for Kv4.3 K^+ channels. *J. Membr. Biol.* 188:73–86.

Goldstein, S.A.N., D.J. Pheasant, and C. Miller. 1994. The charybdotoxin receptor of a *Shaker* K^+ channel: peptide and channel residues mediating molecular recognition. *Neuron*. 12:1377–1388.

Gomez-Lagunas, F. 1997. *Shaker* B K^+ conductance in Na^+ solutions lacking K^+ ions: a remarkably stable non-conducting state produced by membrane depolarizations. *J. Physiol.* 499(Pt 1):3–15.

Harris, R.E., H.P. Larsson, and E.Y. Isacoff. 1998. A permanent ion binding site located between two gates of the *Shaker* K^+ channel. *Biophys. J.* 74:1808–1820.

Haug, T., R. Olcese, L. Toro, and E. Stefani. 2004. Regulation of K1 flow by a ring of negative charges in the outer pore of BK_{Ca} channels. Part II: Neutralization of aspartate 292 reduces long channel openings and gating current slow component. *J. Gen. Physiol.* 124:185–197.

Heginbotham, L., T. Abramson, and R. MacKinnon. 1992. A functional connection between the pores of distantly related ion channels as revealed by mutant K^+ channels. *Science*. 258:1152–1155.

Heginbotham, L., Z. Lu, T. Abramson, and R. MacKinnon. 1994. Mutations in the K^+ channel signature sequence. *Biophys. J.* 66: 1061–1067.

Hille, B. 2001. Ionic Channels of Excitable Membranes. Third edition. Sinauer Associates Inc., Sunderland, MA. 814 pp.

Horrigan, F.T., and R.W. Aldrich. 1999. Allosteric voltage gating of potassium channels II. Mslo channel gating charge movement in the absence of $Ca^{(2+)}$. *J. Gen. Physiol.* 114:305–336.

Hurst, R.S., L. Toro, and E. Stefani. 1996. Molecular determinants of external barium block in *Shaker* potassium channels. *FEBS Lett.* 388:59–65.

Iino, M., S. Ciani, K. Tsuzuki, S. Ozawa, and Y. Kidokoro. 1997. Permeation properties of Na^+ and Ca^{2+} ions through the mouse epsilon2/zeta1 NMDA receptor channel expressed in *Xenopus* oocytes. *J. Membr. Biol.* 155:143–156.

Jiang, Y., A. Lee, J. Chen, V. Ruta, M. Cadene, B.T. Chait, and R. MacKinnon. 2003. X-ray structure of a voltage-dependent K^+ channel. *Nature*. 423:33–41.

Kirsch, G.E., J.M. Pascual, and C.-C. Shieh. 1995. Functional role of a conserved aspartate in the external mouth of voltage-gated potassium channels. *Biophys. J.* 68:1804–1813.

Kramers, H.A. 1940. Brownian motion in a field of force and the diffusion model of chemical reactions. *Physica*. 7:284–304.

Latorre, R., A. Oberhauser, P. Labarca, and O. Alvarez. 1989. Varieties of calcium-activated potassium channels. *Annu. Rev. Physiol.* 51:385–399.

Loboda, A., A. Melishchuk, and C. Armstrong. 2001. Dilated and defunct k channels in the absence of k(+). *Biophys. J.* 80:2704–2714.

MacKinnon, R., R. Latorre, and C. Miller. 1989. Role of surface electrostatics in the operation of a high-conductance Ca^{2+}-activated K^+ channel. *Biochemistry*. 28:8092–8099.

MacKinnon, R., and C. Miller. 1989. Functional modification of a Ca^{2+}-activated K^+ channel by trimethyloxonium. *Biochemistry*. 28: 8087–8092.

McLaughlin, S. 1989. The electrostatic properties of membranes. *Annu. Rev. Biophys. Biophys. Chem.* 18:113–136.

Molina, A., P. Ortega-Saenz, and J. Lopez-Barneo. 1998. Pore mutations alter closing and opening kinetics in *Shaker* K^+ channels. *J. Physiol.* 509(Pt 2):327–337.

Neyton, J., and C. Miller. 1988a. Discrete Ba^{2+} as a probe of ion occupancy and pore structure in the high-conductance Ca^{2+} activated K^+ channel. *J. Gen. Physiol.* 92:569–586.

Neyton, J., and C. Miller. 1988b. Potassium blocks barium permeation through a calcium-activated potassium channel. *J. Gen. Physiol.* 92:549–567.

Nimigean, C.M., J.S. Chappie, and C. Miller. 2003. Electrostatic tuning of ion conductance in potassium channels. *Biochemistry*. 42:9263–9268.

Press, W.T., B.P. Flannery, S.A. Teukolsky, and W.T. Vetterling. 1992. Numerical Recipes in C: The Art of Scientific Computing. Second edition. Cambridge University Press, Cambridge, UK. 994 pp.

Roux, B. 1997. Influence of the membrane potential on the free energy of an intrinsic protein. *Biophys. J.* 73:2980–2989.

Shealy, R.T., A.D. Murphy, R. Ramarathnam, E. Jakobsson, and S. Subramaniam. 2003. Sequence-function analysis of the K(+)-selective family of ion channels using a comprehensive alignment and the KcsA channel structure. *Biophys. J.* 84:2929–2942.

Sigg, D., and F. Bezanilla. 2003. A physical model of potassium channel activation: from energy landscape to gating kinetics. *Biophys. J.* 84:3703–3716.

Vergara, C., O. Alvarez, and R. Latorre. 1999. Localization of the K^+ lock-in and the Ba^{2+} binding sites in a voltage- gated calcium-modulated channel. Implications for survival of K^+ permeability. *J. Gen. Physiol.* 114:365–376.

Wallner, M., P. Meera, M. Ottolia, G.J. Kaczorowski, R. Latorre, M.L. Garcia, E. Stefani, and L. Toro. 1995. Characterization of and modulation by a beta-subunit of a human maxi KCa channel cloned from myometrium. *Receptors Channels*. 3:185–199.

Zhou, Y., J.H. Morais-Cabral, A. Kaufman, and R. MacKinnon. 2001. Chemistry of ion coordination and hydration revealed by a K^+ channel-Fab complex at 2.0 A resolution. *Nature*. 414:43–48.